Monthly Notices of the ROYAL ASTRONOMICAL SOCIETY

MNRAS **439,** 3476–3489 (2014)
Advance Access publication 2014 February 27

doi:10.1093/mnras/stu194

Migration of massive black hole binaries in self-gravitating discs: retrograde versus prograde

Constanze Roedig[1,2]★ and Alberto Sesana[1]

[1]*Max-Planck-Institut für Gravitationsphysik, Albert Einstein Institut, Am Mühlenberg 1, D-14476 Golm, Germany*
[2]*Department for Physics and Astronomy, The Johns Hopkins University, 3400 N Charles Street, Baltimore, MD 21218, USA*

Accepted 2014 January 27. Received 2014 January 26; in original form 2013 July 23

ABSTRACT

We study the interplay between mass transfer, accretion and gravitational torques on to a black hole binary migrating in a self-gravitating, retrograde circumbinary disc. A direct comparison with an identical prograde disc shows that: (i) because of the absence of resonances, the cavity size is a factor of $\mathfrak{a}(1+\mathfrak{e})$ smaller for retrograde discs; (ii) nonetheless the shrinkage of a circular binary semimajor axis $\mathfrak{a}$ is identical in both cases; (iii) in line with previous findings, a circular binary in a retrograde disc remains circular while eccentric binaries grow more eccentric. For non-circular binaries, we measure the orbital decay rates and the eccentricity growth rates to be exponential as long as the binary orbits in the plane of its disc. Additionally, for these coplanar systems, we find that interaction ($\sim$ non-zero torque) stems only from the cavity edge plus $\mathfrak{a}(1+\mathfrak{e})$ in the disc, i.e. for dynamical purposes, the disc can be treated as an annulus of small radial extent. We find that simple 'dust' models in which the binary–disc interaction is purely gravitational can account for all main numerical results, both for prograde and retrograde discs. Furthermore, we discuss the possibility of an instability occurring for highly eccentric binaries causing it to leave the disc plane, secularly tilt and converge to a prograde system. Our results suggest that for binaries hardening in self-gravitating discs there are two configurations without further secular eccentricity evolution: the special circular *retrograde* case and an eccentric ($\mathfrak{e} \sim 0.6$) *prograde* configuration as a stable attractor.

Key words: accretion, accretion discs – black hole physics – hydrodynamics – methods: numerical.

1 INTRODUCTION

Supermassive black hole binaries (BHBs)[1] have been predicted to be ubiquitous intermediate products of comparable mass galaxy mergers (e.g. Begelman, Blandford & Rees 1980). Dynamical friction brings the two holes down to ∼pc separation, at which point they feel each other's gravitational pull, forming a Keplerian BHB. If gas is abundant in the nucleus of the merger remnant, strong gas inflows (Mihos & Hernquist 1996) might lead to the formation of a circumbinary disc, therefore providing a natural mean to subtract angular momentum to the binary, possibly driving it to final coalescence (see, e.g. Dotti et al. 2007; Cuadra et al. 2009). Following the seminal work of Goldreich & Tremaine (1980) in the context of planetary dynamics, several studies of subparsec BHBs in gaseous discs (Artymowicz & Lubow 1994; Syer & Clarke 1995; Artymowicz & Lubow 1996; Ivanov, Papaloizou & Polnarev 1999; Gould & Rix 2000; Armitage & Natarajan 2002, 2005; Hayasaki, Mineshige & Sudou 2007; Hayasaki, Mineshige & Ho 2008; MacFadyen & Milosavljević 2008; Cuadra et al. 2009; Hayasaki 2009; Haiman, Kocsis & Menou 2009; Lodato et al. 2009; Lin & Papaloizou 2012; Nixon et al. 2011; Roedig et al. 2011; Shi et al. 2012), employing various techniques, have established the general picture sketched below, for the case in which the BHB and the circumbinary discs are coplanar and corotating. Initially the binary migrates inwards following the 'fluid elements' of the discs (type I) migration. When the local mass of the disc (see e.g. Kocsis, Haiman & Loeb 2012 for a thoughtful discussion) is of the order of the mass of the lighter hole, torques exerted by the binary are strong enough to evacuate the central region of the disc carving a central cavity. Accretion continues on to both holes through the cavity. In the prograde case (studied by the aforementioned papers), the cavity itself has a radius which is about twice the binary separation, and is held up by outer Lindblad resonances (OLR). The gas at the inner edge of the circumbinary disc leaks through the cavity streaming towards either holes. The streams bend in front of each hole and are

★E-mail: Constanze.Roedig@aei.mpg.de

[1] Throughout the paper we always refer to massive/supermassive binaries, we therefore drop the adjective and simply refer to BHBs.

© 2014 The Authors
Published by Oxford University Press on behalf of the Royal Astronomical Society

Downloaded from http://mnras.oxfordjournals.org/ at MPI Gravitational Physics on August 6, 2014

partially gravitationally captured forming *minidiscs*. However, a large amount of gas is flung back out impacting the disc edge, efficiently mediating the disc-binary energy and angular momentum exchange (MacFadyen & Milosavljević 2008; Shi et al. 2012). The semimajor axis, $\mathfrak{a}$, shrinks and the eccentricity, $\mathfrak{e}$, grows and saturates around $\mathfrak{e} \sim 0.6$ (Roedig et al. 2011).

Recently Nixon et al. (2011) investigated the dynamical interaction of BHB embedded in light, non-self-gravitating circumbinary retrograde discs. The absence of OLRs allows the circumbinary disc to survive unperturbed outside the orbit of the binary, with the inner edge impacting directly on to the secondary black hole (BH). So, the retrograde cavity is smaller and there is neither room to accommodate large *minidiscs* nor will there be *stream bending* nor will there be slingshots. The gas at the inner edge is either accreted directly by the secondary hole or loses its energy and angular momentum in the impact when being funnelled on to the primary.

We consider the possibility of a BHB that has migrated to reach parsec separation and is now evolving in a retrograde self-gravitating disc. Without making any a priori statements about the astrophysical likelihood of this scenario (see King et al. 2005; Nixon 2012 for the dynamical conditions under which an accreted gaseous mass will lead to a counterrotating configuration), the first goal of this paper is to make an apple-to-apple comparison of the evolution of the orbital elements of an initially circular BHBs migrating inside pro- versus retrograde discs, to better understand the differences in the physics of the BHB–disc interaction. We demonstrate that, in both configurations, the evolution of the binary elements is well reproduced if the BHB–disc interplay is described in terms of purely gravitational interactions, in which the gas particles are effectively treated as dust. In this picture, the hydrodynamical properties of the disc is only relevant in determining the pace at which gas is supplied for direct interaction with the BHB. This is particularly interesting because it makes our results readily scalable to other astrophysical systems such as protoplanetary discs around young stellar binaries, opening interesting possibilities (that we do not pursue in this paper) for the formation of counterrotating or misaligned planets around binary stars. At very high eccentricity we find hints of an instability that leads to the binary tilting out of the rotation plane of the disc. We pursue this possibility with a dedicated higher resolution simulation and point out the most likely cause of this behaviour. Combining these finding with those of Roedig et al. (2011), we discuss that BHBs in self-gravitating retrograde discs have three possible end stages: (1) a stable circular motion coupled with an orbit decay similar to the aligned state; depending on the stochastic occurrence of the instability either (2) a fast inspiral if the exponential eccentricity growth and semimajor axis decay bring the BHB into the gravitational wave regime or (3) re-alignment of the BHB with its disc and evolution towards the eccentric, prograde standard scenario.

The paper is organized as follows. In Section 2, we describe the numerical method, initial conditions (ICs) and parameters used in our simulations. In Section 3, we provide a compilation of our numerical findings, that we try to explain coherently with a simple model presented in Section 4. The aforementioned tilting instability is studied in Section 5. Concluding, we discuss and summarize the overall findings in Section 6.

2 METHOD

The model and numerical setup of this work is closely related to that of (Roedig et al. 2011, 2012, the latter hereafter Paper I) and Cuadra et al. (2009), hence we only outline the key aspects in the following, and refer the reader to these papers for further details.

2.1 Basic assumptions and caveats

We simulate a self-gravitating gaseous disc of mass $M_{\rm Disc}$ around two BHs of combined mass $M_{\rm BHB} = M_1 + M_2$, mass ratio $\mathfrak{q} = M_2/M_1 \sim 1/3$, eccentricity $\mathfrak{e}$ and semimajor axis $\mathfrak{a}$, using the smoothed particle hydrodynamics (SPH) code GADGET-2 (Springel 2005) in a modified version that includes sink particles which model accreting BHs (Springel, Di Matteo & Hernquist 2005; Cuadra et al. 2006). The disc, which is counterrotating with the BHs, radially extends to about $7\mathfrak{a}$, contains a circumbinary cavity of radial size $\gtrsim \mathfrak{a}$ and is numerically resolved by at least two million particles. The numerical size of each BH is denoted as $r_{\rm sink}$, the radius below which a particle is accreted, removed from the simulation, and its momentum is added to the BH (Bate, Bonnell & Price 1995). The gas in the disc is allowed to cool on a time-scale proportional to the local dynamical time of the disc $t_{\rm dyn} = 2\pi/\Omega_0$, where $\Omega_0 = ({\rm G}M_0/\mathfrak{a}_0^3)^{1/2}$ is the initial orbital frequency of the binary.[2] To prevent it from fragmenting, we force the gas to cool slowly, setting $\beta = t_{\rm cool}/t_{\rm dyn} = 10$ (Gammie 2001; Rice, Lodato & Armitage 2005). This choice of β is discussed in previous work (e.g. Paper I).

It might be argued that in realistic subparsec accretion discs, the actual cooling time-scale is much shorter than what is implied by our cooling prescription, leading to its fragmentation on a dynamical time. We shall, however, consider two things. First, we anticipate that the dynamical evolution of the BHB is entirely determined by the amount of gas feeding the streams and being eventually captured by the two holes. Decreasing the surface density of the disc (stabilizing it) will simply proportionally decrease the amount of gas experiencing a direct interaction with the binary. Typical evolutionary time-scales will thus be longer, but this will not affect the underlying physical differences in the prograde versus retrograde scenario. In practice our main results are readily re-scalable to much lighter discs which are not prone to fragmentation. Secondly, the standard Toomre stability criterion can be written as $M_{\rm Disc}/M_{\rm BHB} \approx H/r$ (Pringle 1981). Although it is true that standard active galactic nuclei discs tend to fragment at few thousands Schwarzschild radii in virtue of their extremely small aspect ratio ($H/r \sim 10^{-3}$; Goodman 2003), much larger masses can be stable against self-gravity if a thicker structure is formed. Our discs have $H/r \approx 0.1-0.2$ in the region where the bulk of the mass is contained, implying a Toomre parameter $Q \approx 1$ for the assumed $M_{\rm Disc}/M_{\rm BHB} \approx 0.13-0.18$. In our simulation this condition is artificially obtained by setting a high sound speed for the adiabatic gas, which implies an unlikely physical disc temperature of 10^6 K. However, our main interest is to set a stable structure, and the artificially high sound speed can be envisaged as a surrogate to mimic a source of vertical support given by some other physics. Along these lines, Gaburov, Johansen & Levin (2012) have shown that accretion of a weakly magnetized massive cloud, results in the formation of a massive disc supported by an ordered magnetic field that sustain a stable vertical structure with aspect ratio $H/r > 0.15$. They compute for that scenario a critical stable mass of the disc of about $0.3M_{\rm BH}$, larger than the mass of our disc.

[2] Subscripts 0 refer to the initial values of any parameter. Throughout the paper, all figures will be shown in code units $\rm G = M_0 = 1$.

Downloaded from http://mnras.oxfordjournals.org/ at MPI Gravitational Physics on August 6, 2014

Table 1. Run labels and initial parameters in code units. The prograde run is taken from Paper I. On a side note: N is the resolution, ** denotes that additional cross-checks were performed to ensure that all conservation laws were numerically satisfied.

Model	$\mathfrak{a}_0$	$\mathfrak{e}_0$	$r_{\rm sink}$	N	$M_{\rm Disc}/M_{\rm BHB}$
pro $\mathfrak{e}=0$	1.0	0.02	0.05	2 M	0.186
count00	0.97	0.02	0.05	3 M	0.13
count01	0.92	0.09	0.05	3 M	0.13
count02	0.83	0.19	0.05	3 M	0.13
count03	0.74	0.30	0.05	3 M	0.13
retro $\mathfrak{e}=0$	1.0	0.02	0.05	2 M	0.186
retro $\mathfrak{e}=0.1$	1.0	0.10	0.05	2 M	0.186
retro $\mathfrak{e}=0.3$	1.0	0.27	0.05	2 M	0.186
retro $\mathfrak{e}=0.5$	1.0	0.46	0.05	2 M	0.186
retro $\mathfrak{e}=0.8$	1.0	0.83	0.05	2 M	0.186
retro** $\mathfrak{e}=0.7$	1.0	0.56	0.05	4 M	0.176
retro** $\mathfrak{e}=0.9$	1.0	0.94	0.04	4 M	0.186

2.2 Discussion of initial conditions

We start the simulations using two different approaches for obtaining ICs, the relevant quantities of which are listed in Table 1. In the standard case, labelled `retro` throughout, a relaxed prograde disc is taken and the orbital angular momentum vector of the BHB, $\mathbf{L}_{\rm BHB}$, is flipped and the eccentricity is changed. To be specific, we took the ICs of model *adia05* in Paper I, in order to facilitate a direct prograde versus retrograde comparison. This prograde run is labelled pro $\mathfrak{e}=0$. Additionally, to measure how fast the memory of any out-of-equilibrium IC is lost and in order to avoid any spurious systematics, the following test was performed: the cavity was filled with gas to form a solid accretion disc lacking any low density region around the BHB. A circular BHB was placed around the centre of mass (CoM) and integrated to measure how many orbits the system would need to relax. We observed an initial transient marked by high accretion and BHB shrinkage that lasted 45 orbits. Thereafter the system converged to a perfectly relaxed behaviour, the evolution of which in terms of *time derivative* of the semimajor axis $\dot{\mathfrak{a}}$, the eccentricity $\dot{\mathfrak{e}}$ and mass, $\dot{M}_{\rm BHB}$, could not be distinguished from the retro $\mathfrak{e}=0$ setup. We thus only show data that exclude the first 45 orbits, to avoid any potential initial transient. Unless otherwise stated, for each setup we use the orbits 45−90 for the analysis. The second set of ICs, labelled `count`, uses a disc that was left to relax on to a retrograde, circular BHB for 750 orbits, which is why the disc is lighter as it got depleted over time. After 750 orbits, we modify the binary semimajor axis and eccentricity, keeping the quantity $\mathfrak{a}(1+\mathfrak{e})$ approximately constant. This is physically motivated by the previous observation that the gap size in a prograde disc is, at zero order, determined by the apocentre of the BHB orbit.[3] We then let the system evolve for 90 orbits and, as in the `retro` case, we keep orbits 45−90 for the analysis. In Fig. 1, we plot the surface densities of all runs (averaging over orbits 45−90). In the top panel we show the `retro` profiles as a function of radius in units of $\mathfrak{a}$. As $\mathfrak{e}$ increases, the edge of the cavity is pushed outwards, and the profile of the disc inside the cavity becomes shallower. The lower panel shows the profiles of the four `count` setups in comparison with the prograde, circular setup, as a function of radius now in units of $\mathfrak{a}(1+\mathfrak{e})$. For the `count` runs $\Sigma(r)$ are very similar and the radial displacement in $\Sigma_{\rm max}$ between prograde and retrograde is one semimajor axis (i.e. the disc extends inwards because of lack of resonances). In Fig. 2, the logarithmic surface density inside $5\mathfrak{a}$ is shown for the two runs retro $\mathfrak{e}=0$ and retro $\mathfrak{e}=08$, with colour code and scale identical to Paper I, fig. 9. We can appreciate here the much smaller and well-defined cavity in the circular case compared to the eccentric one.

[3] In reality, in the prograde case, we observed the gap size to be slightly larger than $2\mathfrak{a}(1+\mathfrak{e})$ due to non-accreted gas being flung out in a slingshot, impacting at the gap edge, shocking and pushing the edge further outwards. In the retrograde setup, we do not expect slingshots to play any role.

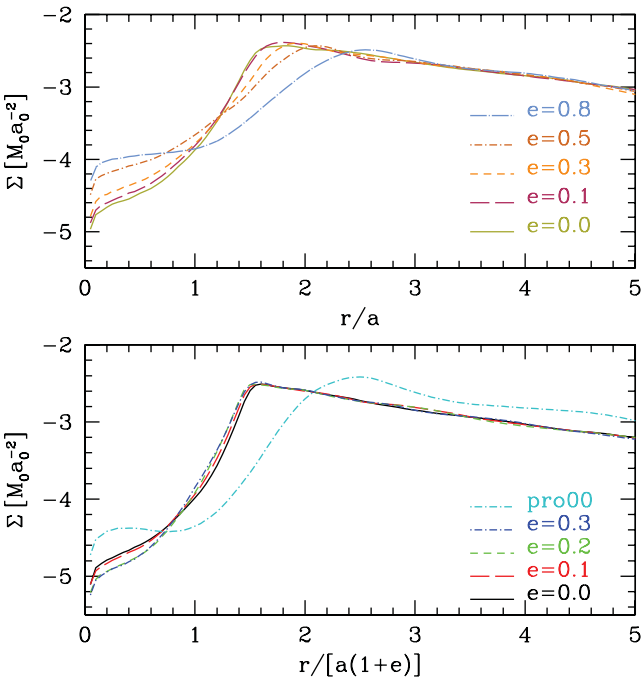

Figure 1. Retrograde runs, average surface density $\Sigma(r)$. Top: "`retro` runs. Bottom: constant $(1+\mathfrak{e})\mathfrak{a}$ runs "`count`" runs, Additionally, the circular prograde case is overlaid, in which the surface density peaks at a radius that is 1 $\mathfrak{a}$ larger than in the retrograde case. Note that $M_{\rm Disc}$ in the `count` runs is smaller than in the `retro` runs. See text for more details; quantities are in code units.

The question of the necessary resolution is addressed both by changing the total number of SPH particles and by changing the mass of each SPH particle (thus giving a different disc thickness, which must be sufficiently sampled). As can be seen by inspecting Table 1, the `retro` runs use 2, the `count` runs use 3 and the `retro`** runs use four million particles (where we state the resolution *after* discarding relaxation). We measured differential torque densities, $\mathrm{d}T_{\mathrm{G},z}/\mathrm{d}r$ (see Section 3.2), per unit mass in retro $\mathfrak{e}=0$ versus `count00`, and found small, but no significant differences between the averaged torques for the circular runs. This assures us that the resolution is sufficient in the `retro` runs, that the results are not sensitive to the precise choice of disc mass and that the relaxation of the discs to the new BHB orbit is fast (the `count00` run effectively discards the first 795 orbits of relaxation at which time it has a resolution of three million). To be conservative, we use four million particles and monitor closely all conservation laws for the more complex dynamical geometry discussed at the end of the paper.

Downloaded from http://mnras.oxfordjournals.org/ at MPI Gravitational Physics on August 6, 2014

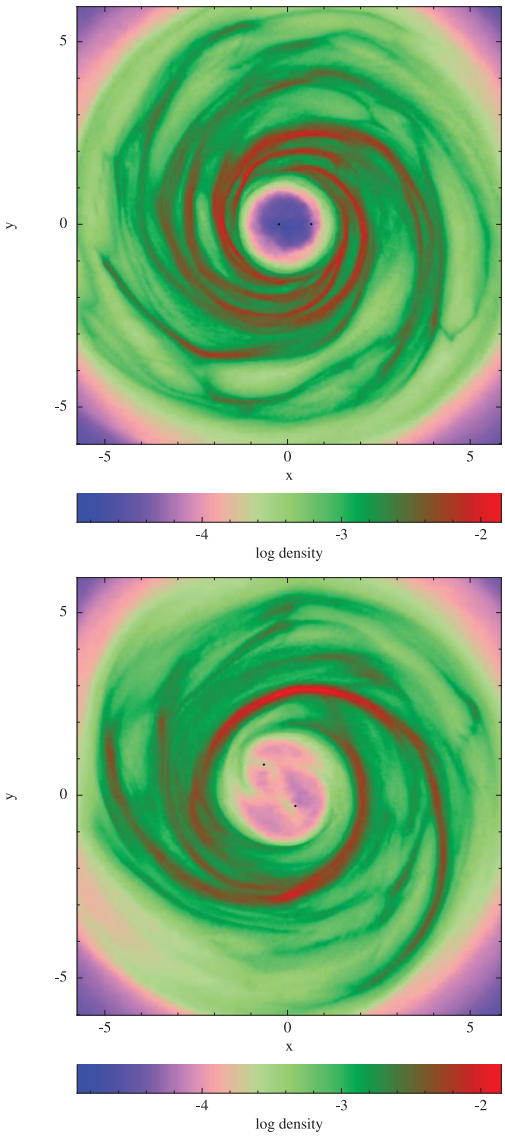

Figure 2. Disc surface density of runs `retro` $\mathfrak{e} = 00$ (top) and `retro` $\mathfrak{e} = 08$ (bottom). Colours are in log–density scale as indicated by the colour bars, all plots are in code units $G = M_0 = \mathfrak{a}_0 = 1$ and snapshots are taken at the same time $t = 70$.

3 ANALYSIS OF THE NUMERICAL DATA

3.1 Binary evolution: general features

We start with a qualitative description of the several outputs of the simulations. In Fig. 3, we show the measured evolution of the individual accretion rates $\dot{M}_1$, $\dot{M}_2$, semimajor axis $\mathfrak{a}$ [for clarity normalized to $\mathfrak{a}(t = 45)$] and the eccentricity $\mathfrak{e}$ for all the `retro` runs. The circular prograde case is shown in the top-left panel for comparison. For the highest $\mathfrak{e}$, we add a panel showing the inclination i[4] in degrees; 180° implies perfect anti-alignment [an additional line shows the inclination $i_{2.5}$ of only the material inside of $r < 2.5\mathfrak{a}(1 + \mathfrak{e})$]. In all cases $\langle \dot{\mathfrak{a}} \rangle < 0$ (here and in the following $\langle * \rangle$ indicates time average) and its absolute value increases with eccentricity; i.e. more eccentric counterrotating binaries appear to shrink faster. $\langle \dot{\mathfrak{e}} \rangle$ is positive for $\mathfrak{e} > 0$, but it is almost exactly zero for the quasi-circular run (`retro` $\mathfrak{e} = 0$). This is in contrast to the circular prograde case, which features $\langle \dot{\mathfrak{e}} \rangle > 0$ (top-left panel). The accretion rate on to each hole is comparable in the `retro` $\mathfrak{e} = 0$ and it is smaller than the prograde case. With increasing $\mathfrak{e}$, the accretion on to the secondary hole becomes larger and highly periodic (modulated on the orbital period of the binary). The `retro` $\mathfrak{e} = 0.8$ case shows a different general behaviour. The binary leaves the disc orbital plane, making accretion on the primary hole easier (the secondary hole does not 'screen' the primary anymore) and the eccentricity growth has a turnover at $\mathfrak{e} = 0.9$. We will return on this latter run extensively in Section 5.

3.2 Gravitational and accretion torques

As elucidated in Paper I the evolution of the binary elements is driven by the sum of the gravitational plus the accretion torques: $\dot{\mathbf{L}}_{\rm BHB} = \mathbf{T}_{\rm G} + \mathbf{T}_{\rm acc}$.[5] The total gravitational torque exerted by the sum of the gaseous particles on each individual BH can be computed as

$$\mathbf{T}_{\rm G} = \sum_{j=1}^{N} \sum_{k=1}^{2} \mathbf{r}_k \times \frac{{\rm G} M_k m_j (\mathbf{r}_j - \mathbf{r}_k)}{|\mathbf{r}_j - \mathbf{r}_k|^3}, \tag{1}$$

where $\mathbf{r}$ is the position vector with respect to the system CoM. The accretion torque $\mathbf{T}_{\rm acc}$ is measured from the conservation of linear momentum in the accretion process of each particle, i.e. $\mathbf{T}_{\rm acc} = \mathbf{r}_k \times m_j \mathbf{v}_j$ (here $\mathbf{r}_k$ is the position vector of the accreting BH, and m_j and $\mathbf{v}_j$ are the mass and velocity of the accreted gas particle). In the following, all torques are averaged both in time and azimuth. In all `retro` runs, we use a reference frame in which the angular momentum of the disc, $\mathbf{L}_{\rm disc}$, is initially aligned to the z-axis and points in the positive z-direction, whereas $\mathbf{L}_{\rm BHB}$ points in the negative z-direction. Assuming that the binary and the disc are coplanar, the system is effective 2D from the dynamical standpoint. We can therefore safely take $\mathbf{L} \approx L_z$ and $\mathbf{T} \approx T_z$, and unless otherwise specified, we will always refer to the z components of these quantities.[6]

As discussed in the previous section, the natural scale of the system is the apocentre distance of the BHB. We thus integrate the differential torques both in- and outwards of $\mathfrak{a}(1 + \mathfrak{e})$ as

$$\langle T_{z,[a,b]} \rangle = \left\langle \int_a^b \frac{{\rm d}T_z}{{\rm d}r} {\rm d}r \right\rangle. \tag{2}$$

In Fig. 4, we show the differential, gravitational torque ${\rm d}T_{{\rm G},z}/{\rm d}r$ on the primary BH (red), on the secondary BH (green), the sum of the two (blue) and the total integrated torque (black). In opposition to the prograde case, the figure clarifies that the interaction between the disc and the binary takes place mostly at the location of the secondary, supporting a direct 'BH–gas impact' model, as described by Nixon et al. (2011). The differential torque density, ${\rm d}T_{{\rm G},z}/{\rm d}r$, of the runs `pro` $\mathfrak{e} = 0$ and `retro` $\mathfrak{e} = 0$ is shown in Fig. 5, where the leftmost panels show the total ${\rm d}T_{{\rm G},z}/{\rm d}r$ on the binary, the middle panel the torque density on to the primary BH and the right, on to the secondary BH. Here, we can clearly appreciate the absence of a gap between $\mathfrak{a}$ and $2\mathfrak{a}$ in the retrograde run. The lower-left panel highlights the unbalanced positive torque (blue) at the location of

[4] Defined as $i = \arccos\left(\frac{\langle \mathbf{L}_{\rm BHB} | \mathbf{L}_{\rm Disc} \rangle}{|\mathbf{L}_{\rm BHB}||\mathbf{L}_{\rm Disc}|}\right)$.

[5] Throughout the paper we use boldface for vectors.

[6] This does not apply to the `retro` $\mathfrak{e} = 0.8$ case that will be discussed separately in Section 5.

Downloaded from http://mnras.oxfordjournals.org/ at MPI Gravitational Physics on August 6, 2014

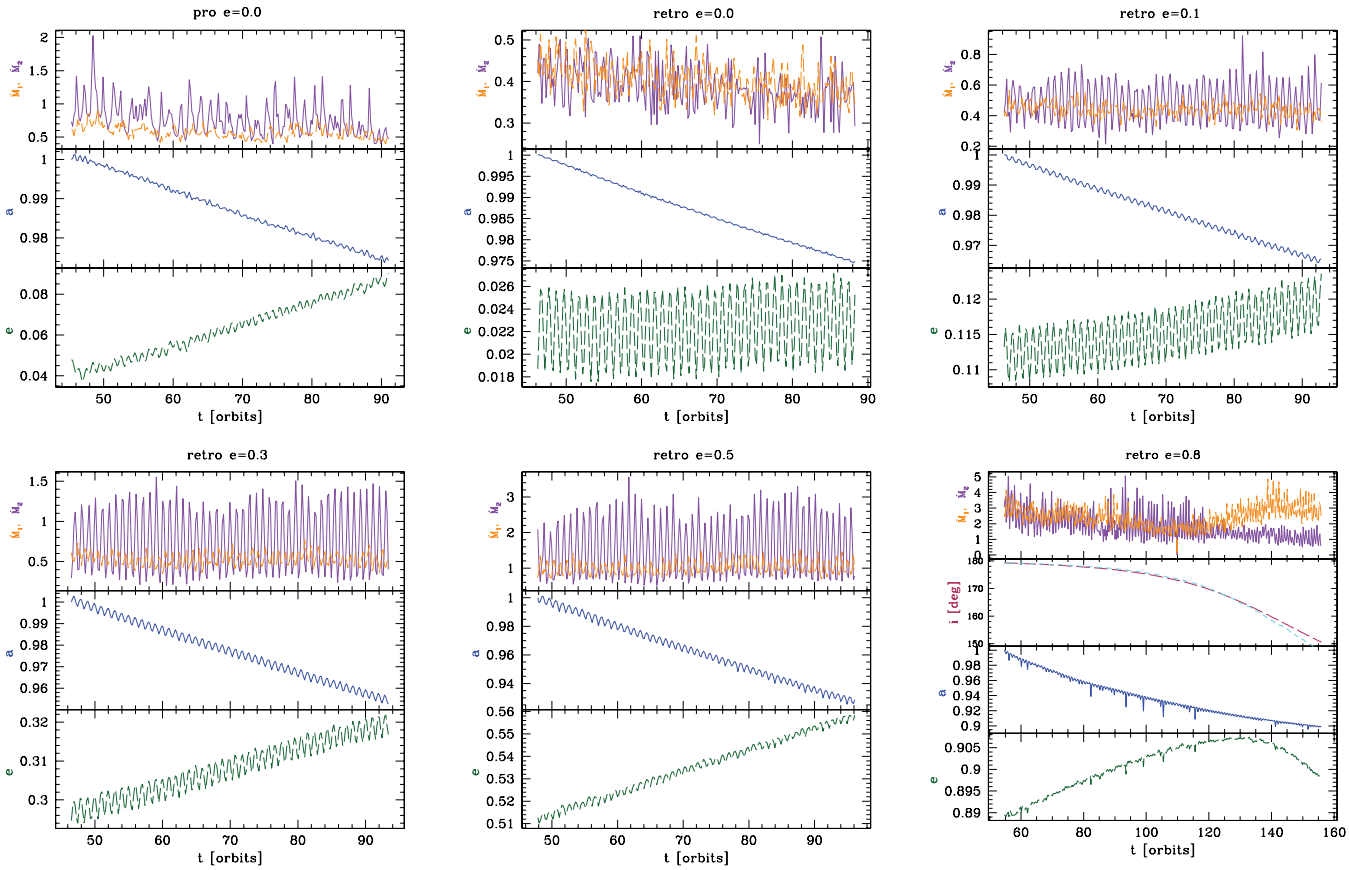

Figure 3. Evolution of the accretion rates, semimajor axis, eccentricity and inclination. All `retro` runs are shown, as indicated above each panel. We also show the prograde run in the top-left panel. In each panel we plot the individual accretion rates $\dot{M}_1$, $\dot{M}_2$ (multiplied by 10^5), the semimajor axis $\mathfrak{a}$ and the eccentricity $\mathfrak{e}$. In the `retro` $\mathfrak{e} = 0.8$ panel we also include the relative BHB–disc inclination i in degrees. Note the different scales on the y-axis; quantities are in code units.

the secondary hole, which is responsible for the binary evolution. (Note, that the orbital angular momentum of the binary is negative in the `retro` runs.)

Differentiating $\mathbf{L}_{\rm BHB}$ with respect to the relevant binary elements, angular momentum conservation yields

$$\frac{\dot{\mathfrak{a}}}{\mathfrak{a}} = \frac{2\,T_{\rm G_z}}{L_z} + \frac{2\,T_{\rm acc_z}}{L_z} - \frac{\dot{M}}{M} - \frac{2\dot{\mu}}{\mu} + \frac{2\mathfrak{e}}{1-\mathfrak{e}^2}\dot{\mathfrak{e}}, \tag{3}$$

where $\mu = M_1 M_2/M$ is the binary reduced mass. Note that all quantities in equation (3) can be directly measured from the simulation outputs. We can therefore use it to get an empirical measurement on how the angular momentum exchange is redistributed among the relevant binary elements. We have cast equation (3) in terms of the shrinkage rate and shown in Fig. 7 that the two major contributions are $\frac{2\,T_{\rm G_z}}{L_z}$ and $\frac{2\mathfrak{e}}{1-\mathfrak{e}^2}\dot{\mathfrak{e}}$ which are of opposite sign and intrinsically coupled with each other. From this decomposition (cast in terms of the orbital element of choice) we can get a heuristic understanding of the BHB–disc coupling, which will serve as a guide for an analytical interpretation of the results.

3.3 Comparison of circular runs: prograde versus retrograde phenomenology

As we chose the setup of the `retro` runs to be the same as those of the *adia05* run of Paper I, we can compare the evolution of $\mathfrak{a}$ and $\mathfrak{e}$ directly. In Fig. 6, we thus plot the circular runs `retro` $\mathfrak{e} = 0$ versus`pro` $\mathfrak{e} = 0$. The evolution of $\mathfrak{a}$ is not distinguishable over the 45 orbits that we show; on the other hand, the eccentricity behaviour is different, such that $\dot{\mathfrak{e}}|_{\rm retro} = 0$ whereas $\dot{\mathfrak{e}}|_{\rm pro} > 0$. Upon inspecting Fig. 3, we find that also the accretion rates for the prograde setup are larger and that while the individual rates are equal for the retrograde, the secondary BH accretes and varies more in the prograde. Considering now the very left-hand panels of Fig. 4, focusing only on the gravitational *inwards* torque, $T_{{\rm in},\,z}$, we find them to be very similar, but opposite in sign with respect to $L_{{\rm BHB},\,z}$. However, the integrated $T_{{\rm in},\,z}$ is slightly smaller in the prograde and there are three clear differences, which are directly related to the absence of OLRs (Papaloizou & Pringle 1977):

(i) the radial location of largest (differential) torque amplitude on to the individual holes are displaced by a factor of $\mathfrak{a}$;

(ii) the largest peak of the (differential) torque on to the binary (blue dashed line) is around $r \sim 1.7\mathfrak{a}(1+\mathfrak{e})$, (coinciding with the first OLR) where the torques on to the individual holes are in phase, is absent in the retrograde case;

(iii) the substantial *outwards* torques found in the prograde case are completely absent in the retrograde case.

Note that, integrated across the whole r range, the total torques on the binary always have opposite sign with respect to the orientation of $\mathbf{L}_{\rm BHB}$, causing a net transfer of angular momentum from the binary to the disc *both in the prograde and in the retrograde case*. Turning to the redistribution of the angular momentum transfer among the binary elements as detailed by equation (3), we show

Downloaded from http://mnras.oxfordjournals.org/ at MPI Gravitational Physics on August 6, 2014

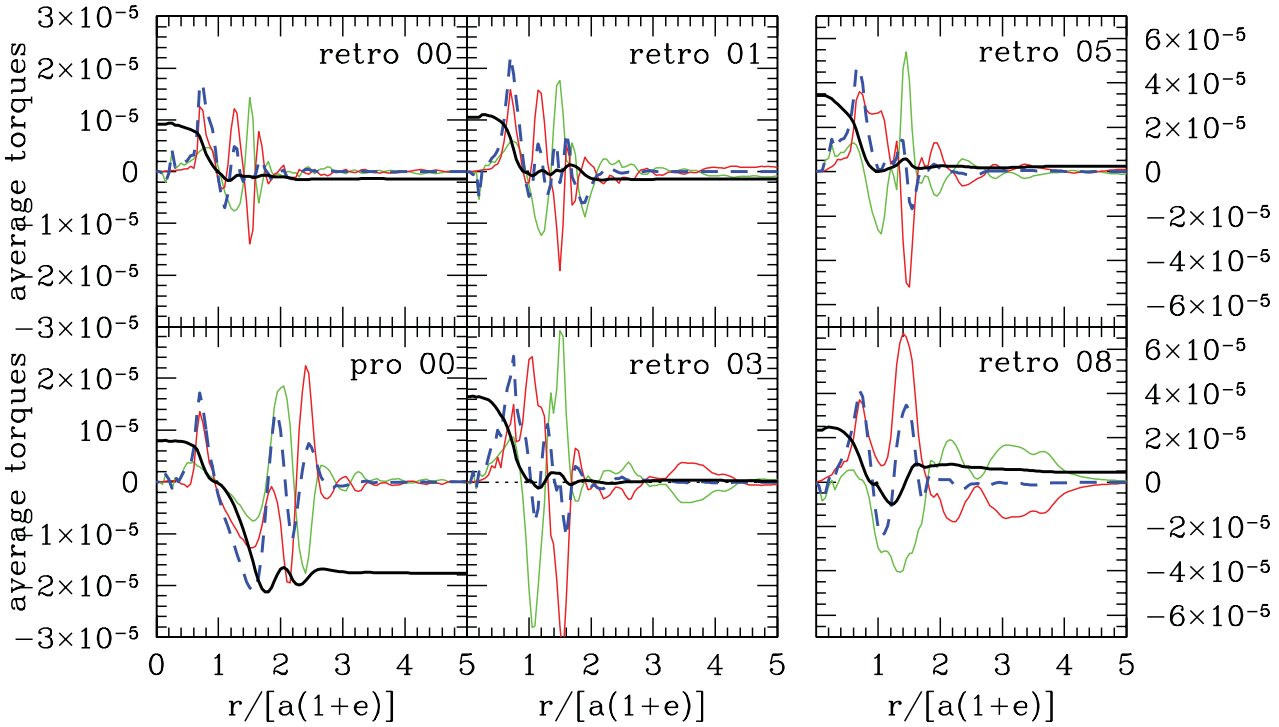

Figure 4. Gravitational torques as a function of the distance to the BHB CoM. In each panel the differential torques $\mathrm{d}T_{\mathrm{G},z}/\mathrm{d}r$ exerted by the disc on to the BHs are averaged over the orbits 45–90 and shown in units of $[\mathrm{G}M_0^2(\mathfrak{a}(1+\mathfrak{e}))^{-2}]$. We show the differential torque on the primary (red), on the secondary (green), the sum of the two (dashed–blue), and the total torques integrated *inwards* and *outwards* (black). Note that the angular momentum of the BHB is negative for retrograde runs and positive for prograde runs. See text for details.

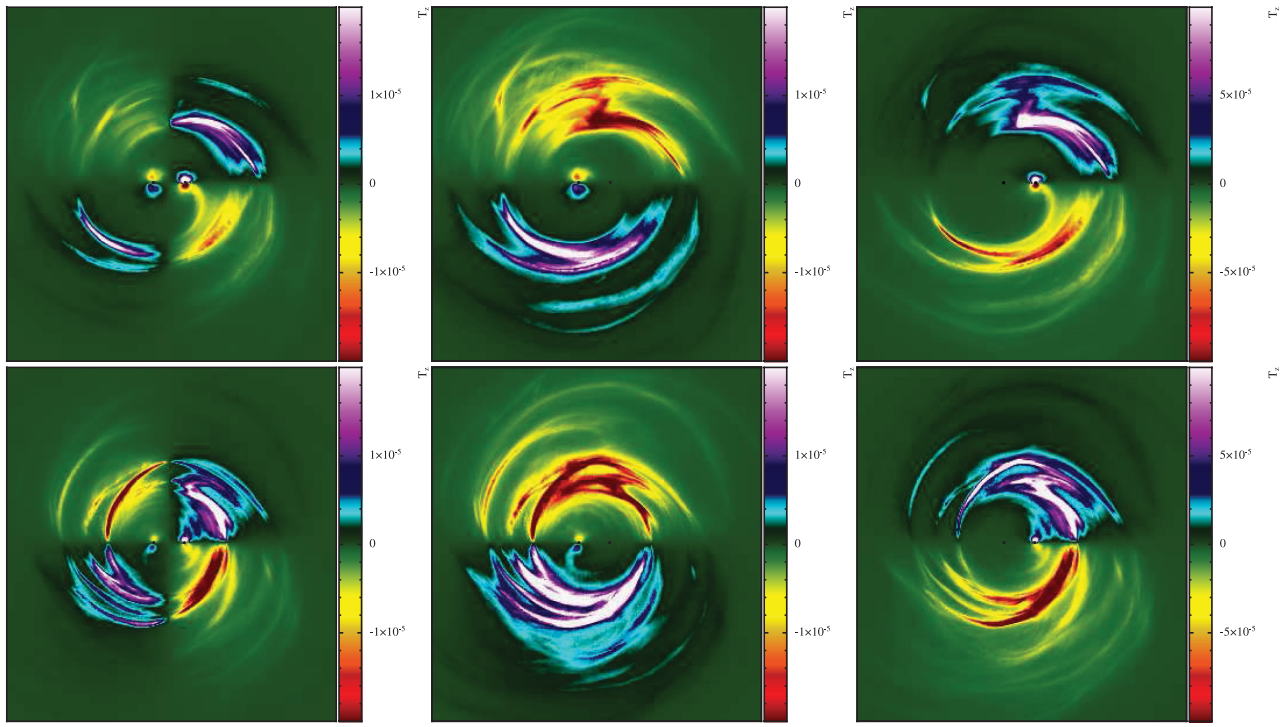

Figure 5. Gravitational torque density. Differential torque density in the z-direction for two initially circular BHB runs after 70 orbits. Top (bottom) panels: `pro` $\mathfrak{e}=0$ (`retro` $\mathfrak{e}=0$). In each row, from left to right we show the total torque density on the binary $T_{\mathrm{G},z}=M_1\,T_{\mathrm{G},z_1}+M_2\,T_{\mathrm{G},z_2}$, the torque on to the primary BH, T_{G,z_1}, and the torque on to the secondary BH, T_{G,z_2}. Figure made using SPLASH (Price 2007).

Downloaded from http://mnras.oxfordjournals.org/ at MPI Gravitational Physics on August 6, 2014

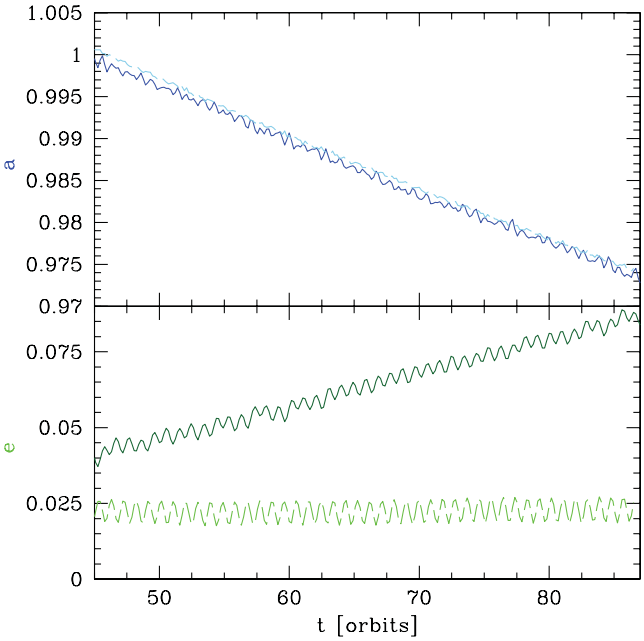

Figure 6. Evolution of semimajor axis and eccentricity for circular BHBs - Direct comparison of the prograde (solid lines) and retrograde (dashed lines) systems. Only the stage after the initial transient is shown. The evolution of $\mathfrak{a}$ cannot be distinguished between the two setups, whereas the evolution of $\mathfrak{e}$ is substantially different.

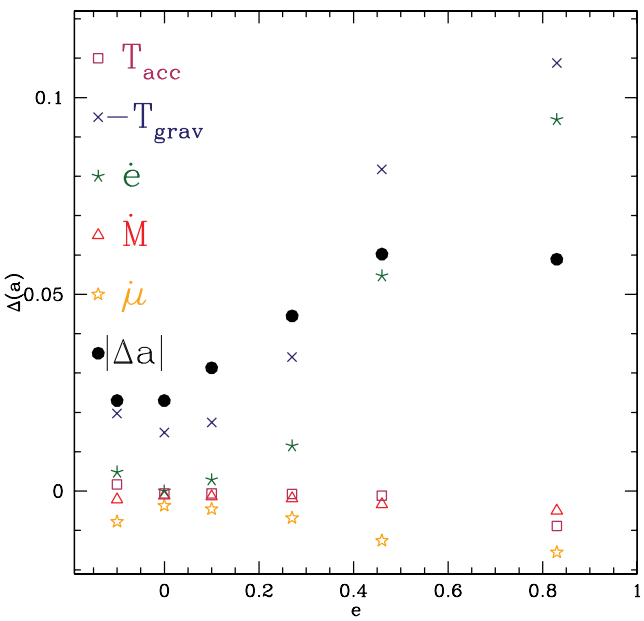

Figure 7. Contributions to $\dot{\mathfrak{a}}$ by individual components; the `pro00` run is inserted as negative $\mathfrak{e}$. Terms colour-coded according to equation (3).

the individual terms from the perspective of $\dot{\mathfrak{a}}$ in Fig. 7 and first compare the two leftmost (i.e. circular) runs.[7] We observe that

(i) the contribution of $\frac{2\mathfrak{e}}{1-\mathfrak{e}^2}\dot{\mathfrak{e}}$ (filled pentagons) is negligible for the retrograde as $\dot{\mathfrak{e}} = 0$

(ii) $2\,T_{\mathrm{acc},\,z}/L_z$ (open squares) contributes negatively for the retrograde, whereas positively (and three times stronger) for the prograde. The sign simply reflects the sign of L_z.

(iii) the mass transfer factors $2\,\dot{\mu}/\mu$ and $\dot{M}/M$ are larger by a factor of ∼2 in the prograde case.

(iv) summing up all components gives a very similar $\dot{\mathfrak{a}}$.

Taken together, these points show that for the retrograde case, the gravitational torque is indeed directly related to the binary semimajor axis evolution, given that the distribution of angular momentum among the other elements of the binary (mass, mass ratio and eccentricity) is negligible.

3.4 Eccentric runs

We turn now to the description of the phenomenology of eccentric runs. In the following, we provide some analytical fits to the few measured data points provided by our set of five simulations ($\{$`retro` $\mathfrak{e} = 0\ \mathfrak{e} = 0.1\ \mathfrak{e} = 0.3\ \mathfrak{e} = 0.5\ \mathfrak{e} = 0.8\}$). We note that sometimes either the circular or the tilting run ($\mathfrak{e} = 0.8$) had to be excluded, and we caution that the fitting functions have only few degree of freedom less than the number of sample points, which is why we do not pursue any extrapolation or other use of the numerical fit coefficients.

In Fig. 4, we plot the evolution of the torque structure from circular to eccentric, and in Fig. 7 the contributions to the shrinkage rate, $\dot{\mathfrak{a}}$ are given, also using the total integrated torque components. Clear trends with increasing $\mathfrak{e}$ are:

(i) with the exception of the run `retro` $\mathfrak{e} = 0.8$, the integrated *inward* torque grows with $\mathfrak{e}$ as

$$T_{\mathrm{in},z}(\mathfrak{e}) \approx T_{\mathrm{in},z}(\mathfrak{e}=0) + 10 \cdot T_{\mathrm{in},z}(\mathfrak{e}=0)\,\mathfrak{e}^2; \tag{4}$$

(ii) the integrated *outward* torque grows linearly with $\mathfrak{e}$, for $\mathfrak{e} \neq 0$, but is always negligible with respect to the *inward* torque;

(iii) a positive *bump* appears in the *outward* torque around $r \sim 1.5\mathfrak{a}(1+\mathfrak{e})$, for $\mathfrak{e} \neq 0$;

(iv) the amplitude of the differential torques, $\mathrm{d}T_{\mathrm{G},\,z}/\mathrm{d}r$, grows with $\mathfrak{e}$;

(v) the maximum radius outside of which $\mathrm{d}T_{\mathrm{G},\,z}/\mathrm{d}r \sim 0$ is approximately $r_{\max} \lesssim 2.5\mathfrak{a}(1+\mathfrak{e})$ (cf. dashed blue lines);

(vi) `retro` $\mathfrak{e} = 0.8$ shows a qualitatively different torque structure, namely there is a large differential torque outside of $r = \mathfrak{a}(1+\mathfrak{e})$, there is a high and positive net torque resulting from the fact, that now *pairs of two* subsequent individual, differential torques (either red or green) alternate in sign, rather than *single* peaks alternating after every extreme (all other panels). We conjecture, that this reflects the BHB leaving the plane of the disc; an effect that will be discussed further in Section 5.

Measuring the derivatives of the orbital elements as a function of $\mathfrak{e}$, we additionally find (cf. Figs 8 and 9):

(i) the dependence of $\dot{\mathfrak{e}}(\mathfrak{e})$ (as long as the inclination stays zero) is linear and positive:

$$\dot{\mathfrak{e}}(\mathfrak{e}) \approx -0.0034 + 0.09\,\mathfrak{e} \tag{5}$$

implying a threshold eccentricity of $\mathfrak{e} \sim 0.04$, for where the growth of $\mathfrak{e}$ would be excited;

(ii) the dependence of $\dot{\mathfrak{a}}(\mathfrak{e})$ is linear and negative;

(iii) the dependence of $\dot{M}_{\mathrm{BHB}}(\mathfrak{e})$ is linear and positive;

(iv) the dependence of $\dot{M}_2/\dot{M}_1(\mathfrak{e})$ is a concave parabola with a best-fitting maximum around $\mathfrak{e} \sim 0.43$.

[7] The prograde run is inserted at negative $\mathfrak{e}$, just to put it next to its retrograde counterpart.

Downloaded from http://mnras.oxfordjournals.org/ at MPI Gravitational Physics on August 6, 2014

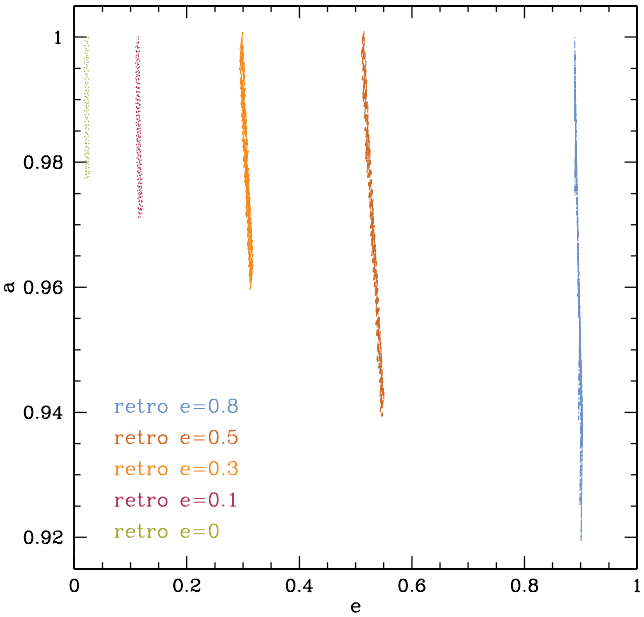

Figure 8. Semimajor axis $\mathfrak{a}$, and eccentricity $\mathfrak{e}$ evolution in the `retro` runs. All runs cover the same time interval. See text for details.

3.5 Accretion rates

In Fig. 3, we can spot clear trends in both $\dot{M}_{\rm BHB}$ and $\dot{M}_2/\dot{M}_1$ with $\mathfrak{e}$. We explore this further in Fig. 9, where we show the accretion rates, both their sum and their ratio, as a function of eccentricity. The combined accretion rate increases with increasing $\mathfrak{e}$, in contrast to what was observed for prograde discs in Paper I. The explanation is straightforward: for prograde runs the cavity is forced to expand with higher $\mathfrak{e}$ due to resonances and slingshots whereas this is not the case for retrograde runs where instead the binary penetrates further and into the disc edge and thus accretes more. Note also that the accretion rate growth is proportional to the enhancement of the inwards torque in Fig. 4 (with the exception of the `retro` $\mathfrak{e} = 0.8$ case), establishing a clear link between the two quantities. The ratio of secondary to primary accretion rate reaches a maximum somewhere in the range $0.4 < \mathfrak{e} < 0.6$ and declines for higher $\mathfrak{e}$. Conversely, in the prograde case (Roedig et al. 2011), the ratio decreases to around $\dot{M}_2/\dot{M}_1 \sim 1$ only for very high $\mathfrak{e} \sim 0.8$ and there is no turnover.

4 ANALYTICAL MODELLING

We now show that the phenomenology described in the previous section can be interpreted in the light of a simple 'dust model' in which particles experience a pure gravitational interaction with the BHB.

4.1 Retrograde runs

The retrograde case has been already described by Nixon et al. (2011, hereafter N11). Following the same argument, we assume that a pure kinetic interaction between the secondary BH and the gas occurs at each apoastron passage. Since in our case $\mathfrak{q} \approx 1/3$, we relax the assumption $\mathfrak{q} \ll 1$, but we keep the ansatz that the inner boundary of the disc interacts with the secondary hole only. A close inspection of the disc–BHB dynamics shows that the gas that 'impacts' on the secondary hole is partly accreted and partly

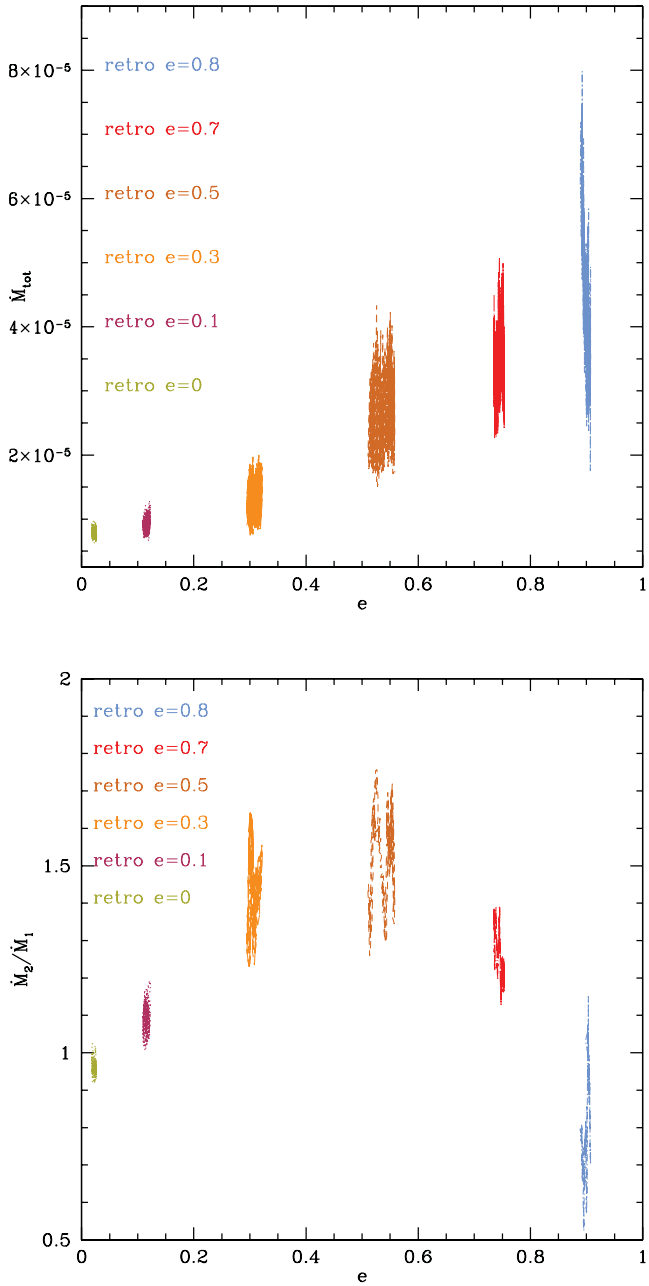

Figure 9. Mass transfer rates as function of eccentricity. Top: total accretion rate for the different runs. Bottom: ratio between secondary and primary accretion rate $\dot{M}_2/\dot{M}_1$, as a function of eccentricity for the retrograde runs. All `retro` runs are plotted over the same time interval (orbits 45−90).

slowed down to the point that is easily captured by the primary. We therefore assume that when a mass ΔM interacts with the secondary, a fraction $0 < \alpha < 1$ is accreted by $M_{\rm BH_2}$, and the remaining $1 - \alpha$ is captured by $M_{\rm BH_1}$. We can therefore impose conservation of linear momentum in the interaction to get (see N11 for the mathematical derivation)

$$\frac{\Delta \mathfrak{a}}{\mathfrak{a}} = -\frac{2\Delta M}{M_2(1+\mathfrak{e})}\mathcal{F}(\mathfrak{e}, \mathfrak{q}, \alpha), \tag{6}$$

$$\Delta \mathfrak{e} = \frac{2\Delta M}{M_2}\mathcal{F}(\mathfrak{e}, \mathfrak{q}, \alpha), \tag{7}$$

Downloaded from http://mnras.oxfordjournals.org/ at MPI Gravitational Physics on August 6, 2014

where

$$\mathcal{F}(\mathfrak{e}, \mathfrak{q}, \alpha) = (1-\mathfrak{e})^{1/2}(1+\mathfrak{q})^{1/2} + \alpha\frac{1-\mathfrak{e}}{1+\mathfrak{q}}, \tag{8}$$

and the $1+\mathfrak{q}$ factors (absent in N11) stem from the fact that we relaxed the condition $\mathfrak{q} \ll 1$. If we now average over the binary orbit, and we take the continuum limit, the above expressions result in two coupled differential equations for $\dot{\mathfrak{a}}$ and $\dot{\mathfrak{e}}$, as a function of the accretion rate $\dot{M}$ and the parameter α. A complete solution to the dynamics requires an additional knowledge of $\dot{M}$ and α as a function of $\mathfrak{a}$ and $\mathfrak{e}$. However Fig. 3 indicates that on the short period of the simulations those are basically constant. We also note that $\mathfrak{e}$ enters in the right-hand side (RHS) of the equations only through the combinations $1-\mathfrak{e}$ and $1+\mathfrak{e}$, providing, over small time-scales, only small corrections that we neglect. We can therefore set $\mathfrak{e} = \mathfrak{e}_0$ in the RHS of equations (6) and (8), perform the integral via separation of variables and linearize the solution to get

$$\mathfrak{a}_t = \mathfrak{a}_0\left[1 - \frac{2\dot{M}}{M_2(1+\mathfrak{e}_0)}\mathcal{F}(\mathfrak{e}, \mathfrak{q}, \alpha)t\right] \tag{9}$$

$$\mathfrak{e}_t = \mathfrak{e}_0\left[1 + \frac{2\Delta M}{M_2}\mathcal{F}(\mathfrak{e}, \mathfrak{q}, \alpha)t\right]. \tag{10}$$

The results are shown in Table 2 for $t = 2\pi \times 45$ (this corresponds to $t = 90$ in Fig. 3). A visual comparison with Fig. 3 indicates that, although there are differences, the overall quantitative agreement is quite good. Discarding the run `retro` $\mathfrak{e} = 0.8$ (the BHB leaves the plane and our analysis does not apply), we notice however that the model slightly underestimate both the binary shrinking and the eccentricity growth for moderate $\mathfrak{e}$ (runs `retro` $\mathfrak{e} = 0.3$, $\mathfrak{e} = 0.5$). If we now approximate the torque exerted on the gas as $T_{\mathcal{G}} = (\mathrm{d}L/\mathrm{d}t)_{\mathcal{G}} \approx -\dot{M}\Delta v_{\mathcal{G}}\mathfrak{a}$ ($v_{\mathcal{G}}$ refers to the gas velocity), and consider that the gas is partly accreted by the secondary (i.e. $\Delta v_{\mathcal{G}} \approx -2v_{M_2}$) and partly slowed down to the point is accreted by M_1 (i.e. $\Delta v_{\mathcal{G}} \approx -v_{M_2}$), we obtain $T_{\mathcal{G}} \approx \dot{M}$ (in simulation units), as observed in Fig. 4. This also trivially explains the behaviour of $T(\mathfrak{e})_{\mathrm{total}}$: for eccentric binaries, the secondary penetrates deeper in the inner rim of the disc, ripping off much more gas, and the torque is simply proportional to $\dot{M}$.

Note that, compared to N11 the systems we consider are substantially different: N11 use 3D SPH with an isothermal equation of state and no self-gravity. A key difference, is that they find mini-discs around the individual BH, which we do not. This must be attributed to the fact, that our gas is allowed to cool proportional to the local dynamical time-scale, whereas their simulations are globally isothermal. Nonetheless the BHB–disc interaction is described by pure gravitational model, which can be applied to a large variety of situations, independently on the particular structure of the disc.

4.2 Prograde run

We put forward a 'dust' model also for the prograde case. As a matter of fact, Lindblad resonances are purely gravitational effects reflecting the fact that no stable hierarchical triplets exist in Newtonian dynamics unless the ratio of the semimajor axis of the inner and the outer binary is larger than a certain value. In our case we can think of the BHB as the inner binary and a gas particle in the disc as the outer body orbiting the CoM of the BHB. The transition between stable and unstable configurations corresponds to the location of the inner edge of the cavity. We can therefore suppose that outside the inner edge, the disc–BHB interaction is weak (as certified by the lower-left panel in Fig. 4). At the inner edge, particles are ripped off and stream towards the binary suffering a slingshot. In a three body scattering, the average BHB–intruder energy exchange in a single encounter is given by (Quinlan 1996; Sesana, Haardt & Madau 2006)

$$\frac{\Delta E}{E} = \frac{2m}{M}C, \tag{11}$$

where $E = -GM_1M_2/(2\mathfrak{a})$ is the binary total energy and m is the mass of the intruder. C is a numerical coefficient of the order of 1.5, which is determined via extensive scattering experiments. Recasting equation (11) in terms of $\mathfrak{a}$ and differentiating, yields

$$\dot{\mathfrak{a}} = -2C\frac{\dot{m}}{M}\mathfrak{a}. \tag{12}$$

However, here $\dot{m}$ is not the accretion rate on to the BHs, but the 'streaming rate' of gas into the cavity, flung back to the disc. We give this number in table 2 of Paper I,[8] and in the adia05 case we get $\dot{m} \approx 5 \times 10^{-5}$. Again, the linear proxy to the solution of equation (12) is simply $\mathfrak{a}_t = \mathfrak{a}_0[1 - 2C\dot{m}t/M]$. If we substitute all the relevant quantities and fix $t = 2\pi \times 45$, we get $\mathfrak{a}_{45} \approx 0.965\mathfrak{a}$. This is about 30 per cent larger than the observed shrink, which is acceptable for such a simple model. The origin of the discrepancy is likely due to dissipation not taken into account here. Part of the streaming gas is actually captured by the hole: in this case, for a particle of mass m the binary acquires a binding energy $-\mathrm{G}Mm/(2R_{\mathrm{cavity}})$ rather than losing an energy given by equation (11) (i.e. $\mathrm{G}m\mu C/\mathfrak{a}$). In our case, $\mu \approx 0.2$. so that the two terms are comparable. Given that ≈25 per cent of the streaming material is accreted, this accounts for the discrepancy. This model also provides an intuitive explanation of the negative torque building up in the region $\mathfrak{a} < r < 2\mathfrak{a}$ in the prograde case. The energy exchange given by equation (11) corresponds to a velocity increment of the gas of the order of $\Delta v_{\mathcal{G}} \approx C\sqrt{2\mathrm{G}\mu/(M\mathfrak{a})}$. Providing a torque on the gas $T_{\mathcal{G}} = (\mathrm{d}L/\mathrm{d}t)_{\mathcal{G}} \approx -\dot{M}\Delta v_{\mathcal{G}}\mathfrak{a}$ (we assume an impulsive interaction at $r = \mathfrak{a}$ and $\boldsymbol{v}_{\mathcal{G}} \cdot \boldsymbol{r} = 0$). This gives, in simulation units a torque acting on the binary of the order $T_{\mathrm{BHB}} = (\mathrm{d}L/\mathrm{d}t)_{\mathrm{BHB}} = -(\mathrm{d}L/\mathrm{d}t)_{\mathcal{G}} \approx 2 \times 10^{-5}$, as observed in the lower-left panel of Fig. 4.

In our simulations, therefore, it makes no significant difference to the shrinking rate whether the BHB is aligned or anti-aligned with its disc. However this appears to be a coincidence residing in the ratio of the ripped-off gas in the corotating case, versus the accreted gas in the retrograde case. Our purely dynamical model does not provide an explanation for this, which stems from the hydrodynamical properties of the gas flow. However, it can be used to quickly determine the evolution of a binary once the in-streaming and accretion rates are known.

Table 2. Analytical model: linearized evolution of the BHB. All `retro` runs are shown. $\mathfrak{a}_{45}$ and $\mathfrak{e}_{45}$ indicate the BHB semimajor axis and eccentricity after 45 orbits of binary evolution, this corresponds to $t = 90$ in Fig. 3.

Model	$\dot{M}(\times 10^{-5})$	α	$\mathfrak{a}_0$	$\mathfrak{a}_{45}$	$\mathfrak{e}_0$	$\mathfrak{e}_{45}$
`retro` $\mathfrak{e} = 0$	0.8	0.50	1.0	0.973	0.022	0.022
`retro` $\mathfrak{e} = 0.1$	1.0	0.52	1.0	0.970	0.112	0.116
`retro` $\mathfrak{e} = 0.3$	1.4	0.58	1.0	0.968	0.297	0.309
`retro` $\mathfrak{e} = 0.5$	2.8	0.60	1.0	0.957	0.511	0.544
`retro` $\mathfrak{e} = 0.8$	5.5	0.44	1.0	0.972	0.888	0.934

[8] Note that in table 2 of Paper I we give the streaming rate per orbital period, not per unit time, the conversion factor is simply 2π.

Downloaded from http://mnras.oxfordjournals.org/ at MPI Gravitational Physics on August 6, 2014

4.3 Accretion rates

We turn now to the observed trends in the accretion rates highlighted in Fig. 9. Those can be understood by comparing the effect of the mass ratio $\mathfrak{q}$ and $\mathfrak{e}$ on the mean distance and relative velocity of the two BHs with respect to the gas at the disc edge. We expect the primary to start accreting much more efficiently as soon as its influence radius at apocentre is equal to the apocentre of the secondary, since in this case the secondary can no longer completely shield the primary from the infalling material. At apocentre, the distances of the BHs to the CoM are $\mathbf{r}_i = \mathfrak{a}(1+\mathfrak{e})/(1+M_i/M_j)$. If indeed accretion is Bondi-like, then the influence radius is given by $r_\mathrm{a} \equiv \mathrm{G}M/(v_\infty^2 + \mathrm{c}_{s,\infty}^2)$, where $v_\infty = v_\mathrm{i} + v_\mathrm{edge}$ and the speeds at apocentre are

$$v_2^2 = \frac{\mathrm{G}M_1}{(\mathfrak{q}+1)\mathfrak{a}}\left(\frac{2}{1+\mathfrak{e}} - 1\right); \quad v_1^2 = \frac{\mathrm{G}M_2\mathfrak{q}}{(\mathfrak{q}+1)\mathfrak{a}}\left(\frac{2}{1+\mathfrak{e}} - 1\right). \tag{13}$$

If we impose a turnover in the relative accretion when $r_1(\mathfrak{e}) + r_{\mathrm{a}_1}(\mathfrak{e}) = r_2(\mathfrak{e})$, and we solve for $\mathfrak{e}$, we get

$$\mathfrak{e}|_\mathrm{t} = \frac{\mathfrak{a}c_s^2(M_2^2 - M_1^2) + \mathrm{G}(M_1^2M_2 + M_1M_2^2 + 2M_2^3)}{[\mathfrak{a}c_s^2(M_1+M_2) + \mathrm{G}M_1(M_1+2M_2)](M_1 - M_2)},$$

which for the average sound speed of our disc, $c_s \approx 0.2$, and $\mathfrak{a} \approx 1$ gives

$$\mathfrak{e}|_\mathrm{t} \sim 0.45. \tag{14}$$

We should mention that the dependence on sound speed, c_s, is not very strong as long as the discs are supersonic. Our discs have Mach numbers between 5 and 10. Additionally, the fact that in the retrograde case for $\mathfrak{e} \gtrsim 0.8$ the ratio $\dot{M}_2/\dot{M}_1$ becomes smaller than unity can be attributed to the fact that the binary leaves the disc plane and starts tilting, so the gas can come closer to the primary without being captured by the secondary.

5 ALIGNMENT BETWEEN THE BHB AND THE DISC PLANE: THE TILTING INSTABILITY

When looking at the bottom-right panel Fig. 3, we find that the inclination of the BHB tilts mildly away from exact anti-alignment ($i = 180$) in the `retro` $\mathfrak{e} = 0.8$ run. At the same time $\mathfrak{e}$ saturates its growth and turns over to become again more circular. In order to study this effect in more detail, we setup the additional run "`retro`$^{**}\mathfrak{e} = 0.9$" with two times the resolution of the default runs and show its orbital element evolution in Fig. 10. Additionally, we monitored the numerical drift of the total angular momentum vector $\mathbf{L}$ to be small and, averaged over an orbit, consistent with a numerical zero. Also, all conservation laws are monitored very closely, and we stop trusting the evolution of "`retro`$^{**}\mathfrak{e} = 0.9$" after orbit 600.

As indicators of the onset of tilting, we identify the following criteria observed in the low-resolution runs:

(i) the ratio of the individual accretion rates would drop below $\dot{M}_2/\dot{M}_1 < 1$;

(ii) the *outward* torque would become significantly positive;

(iii) the individual differential z-torques on to the BHs would stop alternating sign between each peak and rather be pairwise *in phase*;

(iv) the angular momentum (modulus) of the relevant parts of the disc be larger than that of the BHB, i.e. $\mathbf{L}_\mathrm{Disc} > L_\mathrm{BHB}$.

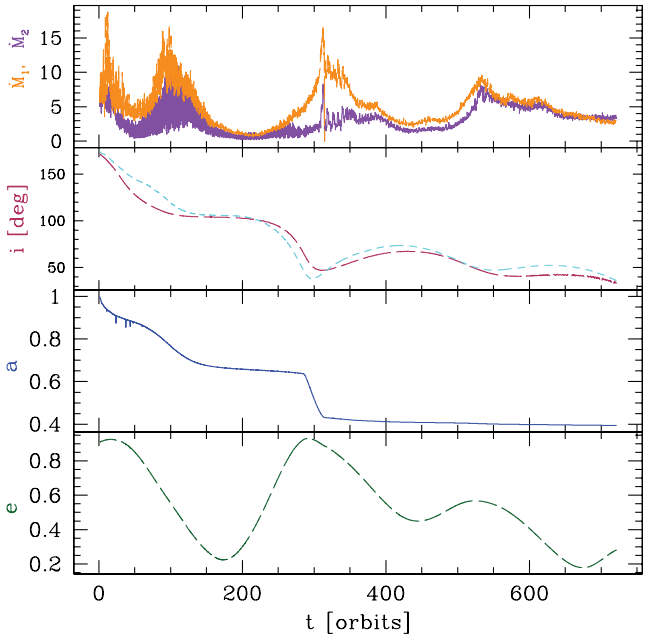

Figure 10. Retrograde high eccentricity run, tilting of the BHB. The "`retro`$^{**}\mathfrak{e} = 0.9$" run; from the top to the bottom, panels show the individual accretion rates $\dot{M}_1$, $\dot{M}_2$ ($\times 1000$), the total inclination i in degrees, the inclination $i_{2.5}$ towards only the inner rings, semimajor axis $\mathfrak{a}$ and the eccentricity $\mathfrak{e}$. See text for more details; quantities are in code units.

We define the relevant angular momentum of the disc to be

$$\mathbf{L}_\mathrm{Disc} \approx \sum_i (\mathbf{r}_i - \mathbf{r}_\mathrm{CoM}) \times \mathbf{p}_i \ , |\mathbf{r}_i - \mathbf{r}_\mathrm{CoM}| < 2.5\mathfrak{a}(1+\mathfrak{e}). \tag{15}$$

Because outwards of this radius, the amplitude of the individual differential torque is essentially zero.[9] While it is true that in order to transport outwards the angular momentum, a radially larger disc is required, the dynamical influence on to the BHB, i.e. the strength and orientation of the torque is given only by the mass and distance of the matter that orbits at radii where the torque is non-zero. For $e > 0.9$ the angular momentum of the BHB drops below $0.5L_\mathrm{Disc}$, which is the condition under which a counteraligned stable configuration is not possible anymore (King et al. 2005). At this point, it should be mentioned, that the two CoM, the one of the BHB and the global CoM exhibit increasing amount of relative movement with $\mathfrak{e}$.

5.1 Physical reasons for the tilting

The retrograde setup differs in several physical properties from the prograde, such that the BHB grazes the disc without the 'stream bending' within the cavity. The appearance of minidiscs is suppressed in the retrograde case, because firstly the cavity is too small to accommodate the discs and secondly because the gas inflows on to the BHs is much more radial than in the prograde case. So the gas is accreted mostly in the wake of the BHs in the retrograde case. Every direct BHB–disc interaction is thus much stronger than in the

[9] Looking at the $t = 1332$ row in Fig. 11, we note that this radius is indeed compatible with the 'warping radius' at which the disc breaks in several differentially precessing annuli. The portion of the disc inside this radius can actively respond to the BHB torques, and is therefore the relevant one for the computation of $\mathbf{L}_\mathrm{Disc}$ (Volonteri, Sikora & Lasota 2007).

Downloaded from http://mnras.oxfordjournals.org/ at MPI Gravitational Physics on August 6, 2014

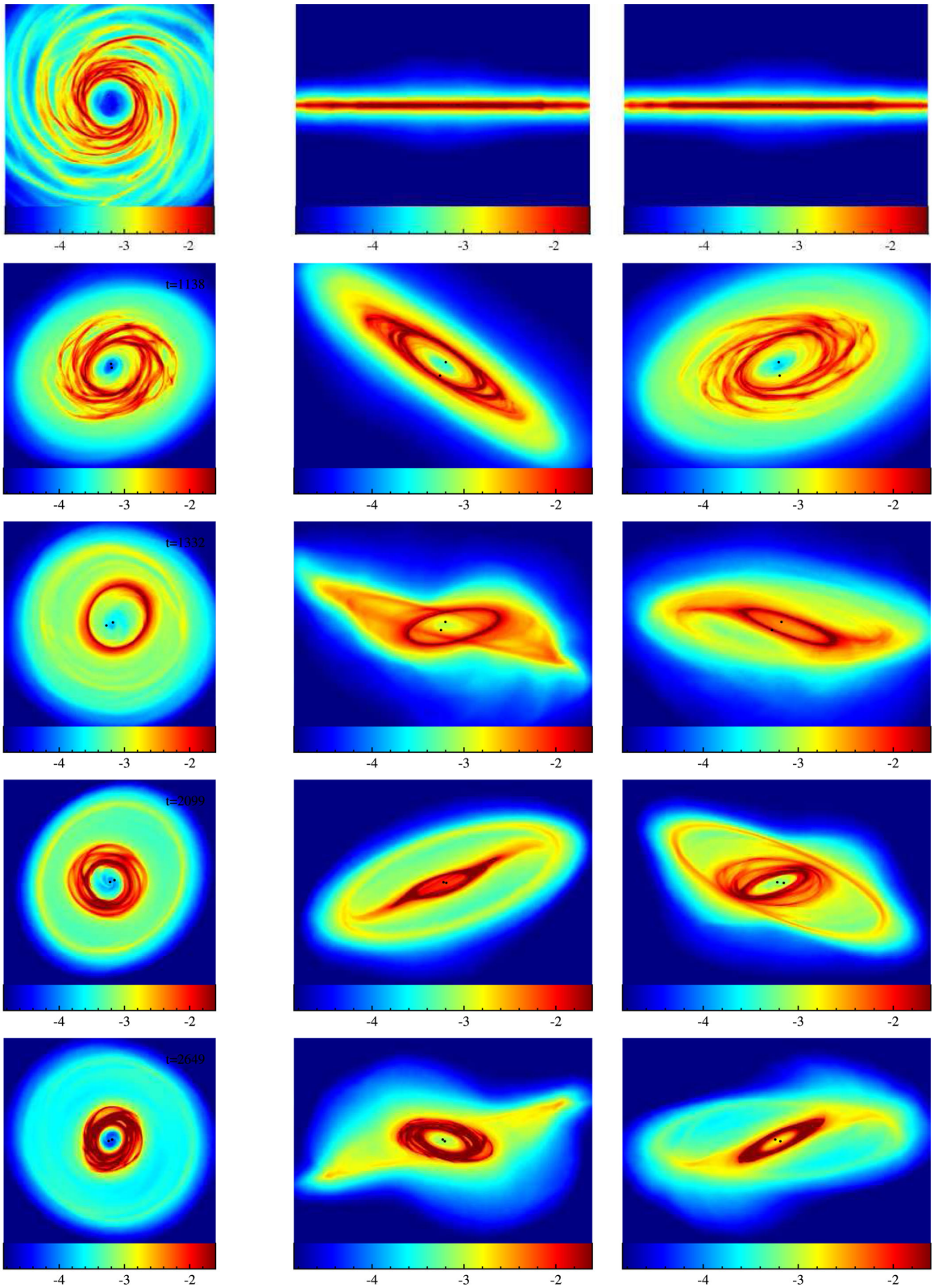

Figure 11. The tilting instability: logarithmic column density, face-on *xy*, edge-on *xz*, edge-on *yz*. Time evolution (top to bottom) of the high accuracy, tilting "`retro`$^{**}\mathfrak{e} = 0.9$" run. Panels show the successive stages of the binary first tilting out of plane and then subsequently aligning with the disc. Note the spread into various annuli that the disc undergoes in the middle panels.

Downloaded from http://mnras.oxfordjournals.org/ at MPI Gravitational Physics on August 6, 2014

prograde case, but takes place in more closely confined space. As $\mathfrak{e}$ increases (and with it $\mathbf{L}_{\rm Disc}/L_{\rm BHB}$) this induces an increasingly large relative movement between the CoM of the BHB with respect to the global CoM. It should be mentioned that the retrograde disc remains circular even if the BHB has high $\mathfrak{e} \sim 0.8$ (cf. Fig. 11, top panel). Thus, it can be understood that the BHB, which has increasingly small angular momentum, has less and less rotational support feeling the impacts into its disc more strongly with increasing $\mathfrak{e}$. The details for a BHB to become secularly unstable to this tilting instability will strongly be disc-model dependent, which is why we only list under which conditions we expect a system to go unstable:

(i) a retrograde disc of $i = 180^\circ$ is an unstable equilibrium configuration if $\mathbf{L}_{\rm Disc} > 2L_{\rm BHB}$ (King et al. 2005) as is the case here: with growing $\mathfrak{e}$ the BHB is increasingly interacting with the retrograde disc, it is not off-hand to expect perturbations that are not perfectly in-plane;

(ii) the corotating case is stable attractor, there should be a threshold value of perturbation that leads the BHB to leave the retroconfiguration in favour of the prograde one;

(iii) if the accretion disc is not perfectly cylindrically symmetric, but rather clumpy and of non-zero vertical extent, perturbations out of plane *and* out of synchronization[10] are well possible.

We shall stress here that while the main results of our in-plane prograde versus retrograde comparison do not depend on the specific value of the disc mass adopted, the tilting instability does. In order to occur, it requires that the disc is massive enough to make the condition $\mathbf{L}_{\rm Disc} > 2L_{\rm BHB}$ possible. On one hand, it is therefore obvious that this effect is not directly observed in simulations where discs are light and self-gravity is not considered (e.g. Nixon 2012; Nixon, King & Price 2013). On the other hand, self-gravitating discs of the required mass might well be prone to fragmentation. As mentioned above, discs of masses $\approx 0.1-0.2 M_{\rm BH}$ might be stable if there is a source of vertical support able to maintain an aspect ratio $H/r > 0.1$. Magnetically levitating accretion discs discussed by Gaburov et al. (2012) provide an example of a structure with aspect ratio $H/r > 0.15$ and critical stable mass $\approx 0.3 M_{\rm BH}$.

5.2 The stages of tilting

We now further explore the tilting itself, assuming that it is a physical effect. The time evolution of this run covers almost 3000 orbits (when taking into account the very significant shrinkage of $\mathfrak{a}(t)$). After an initial increase of $\mathfrak{e}$ there follows circularization which again is followed by an increase in $\mathfrak{e}$. At the same time the inclination i is decreasing then saturating and oscillating until it finally decreases. $\mathfrak{a}$ experiences several phases of strong shrinkage,[11] whereas the accretion rate on to the primary exceeds that on to the secondary until very late times. This behaviour of exchanging inclination and eccentricity is somewhat reminiscent of the Kozai effect.[12] However, it is not straightforward to apply these few body calculations for the BHB–disc scenario studied here: a gaseous disc is not a rigid body and can dissipate angular momentum; nor is the disc a well-located point mass with clearly defined eccentricity and inclination in itself.

The stages that the BHB undergoes on its way towards alignment can be subdivided into the following which are supported by Fig. 11:

(i) *Fast circularization*: the BHB tilts out of plane, $\mathfrak{e}$ quickly shrinks to $\mathfrak{e} \sim 0.2$, while at the same time $\mathfrak{a}$ shrinks almost by a factor of 2.

(ii) *Disc fallback I*: while the BHB has shrunk very fast *and* circularized *and* tilted out of plane, the disc had disintegrated into many annuli of various inclinations due to conservation of angular momentum (see, e.g. Larwood & Papaloizou 1997; Fragner & Nelson 2010; Lodato & Price 2010; Nixon et al. 2012, 2013, for a description of the dynamics of warped discs with a discussion of possible disintegration in precessing annuli and implications for various astrophysical systems). Now, however, the inner part of the gas forms a flat inner disc again. Meanwhile, the gravity torques from the precessing gaseous annuli cause the BHB eccentricity to grow. It should be noted, that the CoM of the BHB and the (inner) disc have drifted apart significantly by now. The accretion rates are low and the semimajor axis remains almost stationary.

(iii) *Inner asymmetric ring collapse*: once the gas has reformed into one (inner) planar disc, the new disc configuration has lost the formerly large BHB upkeeping the cavity size. So, at this point, it re-adjusts to the new BHB 'size' and a hot, dense ring forms (cf. third panel Fig. 11). This ring has very low Toomre parameter, becomes extremely clumpy and the CoM of BHB and disc-ring drift even further apart. Note, that the cooling in the ring depends on the local orbital time-scale. The fallback of gas is accompanied by large accretion rates and thus induced semimajor axis shrinkage. The BHB eccentricity remains very high.

(iv) *Circularization II*: when finally the ring was able to cool enough for its inner part to reach the BHB, the BHB starts circularizing and tilting *into* the disc. The resulting metastable configuration has an inclination of about $i \sim 90^\circ$, is mildly eccentric, a stable semimajor axis and comparatively low accretion rates.

(v) *Disc fallback II*: the initial disc has left behind some outer annuli that now start interacting with the outer part of the (inner) disc. The inner disc and the outer ring are now aligning which is accompanied by a series of precessions of the outer ring. Meanwhile the BHB increases its $\mathfrak{e}$ and stays in the same orientation while the disc tilts towards the BHB.

(vi) *Outer ring collapse*: similar to stage (3), now the outer ring becomes unstable under its own gravity as it has lost too much rotational energy by aligning with the inner disc. (Most of) the outer ring collapses on to the inner disc. The accretion rates are high, but $\mathfrak{a}$ only mildly shrinks.

(vii) *CoM alignment*: once the inner disc and the BHB are the only two major pieces reformed and the inclination is below 60°, the BHB and its new, much more compact disc start aligning their CoMs. This is accompanied by a circularization of the BHB, as during the interaction the BHB pushes the disc towards one side by impacting into it.

[10] Out of synchronization means that the accretion events do not happen coincidentally at the two BHs.

[11] Note, that while energy of the binary shrinks drastically, this is not due to numerical integration error but to the cooling function imposed on the gas. We have verified that at any given moment in the simulation, the numerical energy errors are (about a factor of 10) smaller than the prescribed energy loss of the system.

[12] The Kozai effect (Kozai 1962) is a well known, well-studied phenomenon of a secular three-body interaction when a binary interacts with a perturber that is on an inclined orbit with respect to the binary plane. The perturber can then oscillate in its inclination, pericentre, longitude of ascending node and eccentricity (Takeda, Kita & Rasio 2008) in so-called Kozai cycles. The perturber feels secularly torqued by the binary and starts precessing. Depending on the time-scale of this precession, the binary eccentricity can be excited. For four-body systems, i.e. a binary and two perturbers, the same effect can be found (e.g. Murray & Dermott 1999) where now the two perturbers can additionally exchange inclination and eccentricity.

Downloaded from http://mnras.oxfordjournals.org/ at MPI Gravitational Physics on August 6, 2014

(viii) *Standard* $\mathfrak{e}$*-growth*: when finally the BHB and the disc have re-united their CoMs (apart from a tenuous outer ring), the excitation of $\mathfrak{e}$ similar to what was described in Roedig et al. (2011) starts occurring, while the inclination furthermore decreases.

At the final state of the simulation, the BHB has an inclination of $i \sim 30^\circ$, an eccentricity of about $\mathfrak{e} \sim 0.3$ and the secondary accretion rate is exceeding the primary. During this evolution, the drift of the total angular momentum vector was about 0.8°, and the β cooling has induced a loss of L of about 1.2 per cent. However, we do not trust the evolution past orbit 600, because there appears noise in both the total energy and the total angular momentum and the ratio between $r_{\rm sink}$ and $\mathfrak{a}$ are severely weakening the *inwards* torque, thus vitiating the secular effects drastically. However, from a physical point of view, the aligned, prograde state should be energetically preferred and once the disc has aligned with the BHB, it will be forced to expand its cavity analogously to the prograde case. The numerical problem of performing several thousands of orbits is challenging and we argue here that studying the entire final alignment up to $\mathfrak{e} \sim 0.6$ (cf. Roedig et al. 2011) would be a waste of CPU time, since the physical arguments are quite strong if indeed the instability occurs in the first place.

It is our suspicion that different choices for β, cooling prescriptions, and global disc thermodynamics will alter the 8 stages identified here. The cooling, i.e. the loss of angular momentum seems to be the most crucial numerical parameter in setting the time-scales for the 'ring collapse' and the dissipation of the several annuli.

6 SUMMARY

We presented numerical work on the evolution of the orbital elements of a comparable mass BHB surrounded by a retrograde self-gravitating disc. First, it was found that for quasi-circular BHB–disc configurations, the difference between the retrograde and prograde scenario is chiefly in the eccentricity and mass ratio evolution. The eccentricity remains close to zero in the retrograde case whereas it grows in the prograde case. The semimajor axis shrinkage was found to be the same for the circular BHB irrespective of disc (anti)-alignment. For increasingly eccentric set-ups, the growth of $\mathfrak{e}$ was found to be exponential in time and the coupled evolution of the semimajor axis $\dot{\mathfrak{a}}$ was observed to be proportional to $\mathfrak{e}$(t), thus making the decay very efficient. Additionally, it was found that the individual accretion rates on to the two BHs grow, but that their ratio secondary over primary $\dot{M}_2/\dot{M}_1$ assumes a maximum at eccentricities around $\mathfrak{e} \sim 0.45$.

We demonstrated that all the observed features can be satisfactorily explained using a simple 'dust' model in which the BHB–disc interaction is purely gravitational. In the retrograde case, the absence of resonances together with the high BH–disc relative velocity (i.e. a small cross-section) imply that the gas interacts with the binary only via direct impact on to the secondary. This is confirmed by the fact, that the turnover of $\dot{M}_2/\dot{M}_1(\mathfrak{e})$ could be explained by Bondi–Hoyle like accretion assuming ballistic speeds of disc edge and binary at apocentre. Generalizing the model of N11, we find that this simple 'impact model' is able to catch of the relevant features of the binary evolution at different eccentricities. In the prograde case, the evolution is determined by the gas inflows flung back to the disc. Treating the gas as a dust particle, we found that a simple model based on three body scattering theory fully accounts for the BHB–disc interplay. In those models, however, the mass accretion rate and instreaming rate stem from the hydrodynamical properties of the gas flow and are input parameters.

The retrograde setup shows non-negligible relative motion between the BHB CoM and the global CoM, even in circular runs. In the prograde case, this had been a very small effect only. There are indications that the BHB eccentricity will not grow to $\mathfrak{e} \sim 1$ in the retrograde case, but that the impacts into the disc inner edge destabilize the BHB until it starts moving out of the binary–disc plane. The most important physical conditions for this instability to occur be that the angular momentum of the disc exceed twice that of the BHB and that the disc be sufficiently non-axisymmetric for out-of-plane perturbations to occur. The details of the subsequent alignment are likely to be sensitive to the cooling prescription of the disc, but it is to be expected that the disc disintegrates into several annuli of various inclinations which precess within each other. It was observed that precession of the disintegrated disc annuli causes the BHB eccentricity to grow while the BHB CoM and the disc CoM do not overlap. There were stages wherein the multiple annuli aligned again to try form a coherent, flat disc. Due to loss of rotational support from the shrunk BHB, this was preceded by a short period of fragmentation-like behaviour where the disc collapsed shortly into a dense ring, to spread out into spiral arms later. The BHB eccentricity exhibited few oscillations and it is expected that the final state will be a perfectly aligned disc–BHB system of eccentricity around $\mathfrak{e} \sim 0.6$.

We note, that it is well conceivable that, depending on the physical separation and mass, during any point of the highly eccentric phases the BHB might enter the relativistic regime and rapidly lose energy via gravitational radiation. At this point the circularization effect of gravitational radiation would compete with the eccentricity growth enforced by the retrograde disc, possibly causing a distinctive eccentricity evolution of the system that would be possibly detectable and discernible by low-frequency gravitational wave interferometers (Amaro-Seoane et al. 2013; Consortium 2013), offering an interesting observational test of the BHB–counterrotating disc coupling.

ACKNOWLEDGEMENTS

CR is indebted to Kareem Sorathia, Sarah Buchanan and Rowdy without whom this paper would not have been written. CR is grateful to Julian Krolik and Massimo Dotti for helpful suggestions and was happy to have informative conversations with Cole Miller, Sanchayeeta Borthakur and Jens Chluba. The authors wish to thank the anonymous referee for his/her very constructive comments. All computations were performed on the *datura* cluster of the AEI and CR thanks Nico Budewitz for his HPC support. This work was funded in part by the International Max–Planck Research School, NSF grants AST-0908336, AST-1028111 and the SFB Transregio 7.

REFERENCES

Amaro-Seoane P. et al., 2013, GW Notes, 6, 4
Armitage P. J., Natarajan P., 2002, ApJ, 567, L9
Armitage P. J., Natarajan P., 2005, ApJ, 634, 921
Artymowicz P., Lubow S. H., 1994, ApJ, 421, 651
Artymowicz P., Lubow S. H., 1996, ApJ, 467, L77
Bate M. R., Bonnell I. A., Price N. M., 1995, MNRAS, 277, 362
Begelman M. C., Blandford R. D., Rees M. J., 1980, Nature, 287, 307
Consortium T. E., 2013, preprint (arXiv:e-prints)
Cuadra J., Nayakshin S., Springel V., Di Matteo T., 2006, MNRAS, 366, 358
Cuadra J., Armitage P. J., Alexander R. D., Begelman M. C., 2009, MNRAS, 393, 1423

Downloaded from http://mnras.oxfordjournals.org/ at MPI Gravitational Physics on August 6, 2014

Dotti M., Colpi M., Haardt F., Mayer L., 2007, MNRAS, 379, 956
Fragner M. M., Nelson R. P., 2010, A&A, 511, A77
Gaburov E., Johansen A., Levin Y., 2012, ApJ, 758, 103
Gammie C. F., 2001, ApJ, 553, 174
Goldreich P., Tremaine S., 1980, ApJ, 241, 425
Goodman J., 2003, MNRAS, 339, 937
Gould A., Rix H., 2000, ApJ, 532, L29
Haiman Z., Kocsis B., Menou K., 2009, ApJ, 700, 1952
Hayasaki K., 2009, PASJ, 61, 65
Hayasaki K., Mineshige S., Sudou H., 2007, PASJ, 59, 427
Hayasaki K., Mineshige S., Ho L. C., 2008, ApJ, 682, 1134
Ivanov P. B., Papaloizou J. C. B., Polnarev A. G., 1999, MNRAS, 307, 79
King A. R., Lubow S. H., Ogilvie G. I., Pringle J. E., 2005, MNRAS, 363, 49
Kocsis B., Haiman Z., Loeb A., 2012, MNRAS, 427, 2660
Kozai Y., 1962, AJ, 67, 591
Larwood J. D., Papaloizou J. C. B., 1997, MNRAS, 285, 288
Lin M.-K., Papaloizou J. C. B., 2012, MNRAS, 421, 780
Lodato G., Price D. J., 2010, MNRAS, 405, 1212
Lodato G., Nayakshin S., King A. R., Pringle J. E., 2009, MNRAS, 398, 1392
MacFadyen A. I., Milosavljević M., 2008, ApJ, 672, 83
Mihos J. C., Hernquist L., 1996, ApJ, 464, 641
Murray C. D., Dermott S. F., 1999, Solar System Dynamics. Princeton Univ. Press, Princeton, NJ
Nixon C. J., 2012, MNRAS, 423, 2597
Nixon C. J., Cossins P. J., King A. R., Pringle J. E., 2011, MNRAS, 412, 1591
Nixon C., King A., Price D., Frank J., 2012, ApJ, 757, L24
Nixon C., King A., Price D., 2013, MNRAS, 434, 1946
Papaloizou J., Pringle J. E., 1977, MNRAS, 181, 441
Price D. J., 2007, Publ. Astron. Soc. Aust., 24, 159
Pringle J. E., 1981, ARA&A, 19, 137
Quinlan G. D., 1996, New Astron., 1, 35
Rice W. K. M., Lodato G., Armitage P. J., 2005, MNRAS, 364, L56
Roedig C., Dotti M., Sesana A., Cuadra J., Colpi M., 2011, MNRAS, 415, 3033
Roedig C., Sesana A., Dotti M., Cuadra J., Amaro-Seoane P., Haardt F., 2012, A&A, 545, A127 (Paper I)
Sesana A., Haardt F., Madau P., 2006, ApJ, 651, 392
Shi J.-M., Krolik J. H., Lubow S. H., Hawley J. F., 2012, ApJ, 749, 118
Springel V., 2005, MNRAS, 364, 1105
Springel V., Di Matteo T., Hernquist L., 2005, MNRAS, 361, 776
Syer D., Clarke C. J., 1995, MNRAS, 277, 758
Takeda G., Kita R., Rasio F. A., 2008, in van de Hulst H. C., ed., Proc. IAU Symp. 4, Radio Astronomy. Cambridge Univ. Press, Cambridge, p. 181
Volonteri M., Sikora M., Lasota J.-P., 2007, ApJ, 667, 704

This paper has been typeset from a TEX/LATEX file prepared by the author.

Downloaded from http://mnras.oxfordjournals.org/ at MPI Gravitational Physics on August 6, 2014